Measurement of the Milky Way's Rotation Curve and Calculation of Its Mass and Density Distributions

H. Islam* and E. Davis†
University of New Hampshire, Durham, NH, 03824, USA
(Dated: November 14, 2020)

We use the Small Radio Telescope (SRT) at the University of New Hampshire to measure the orbital velocities of neutral hydrogen clouds at galactic longitudes ranging from 10° to 90° and plot the rotation curve. We find that the rotation curve is mostly flat outside of the central region, corresponding a to a mass distribution that does not follow the luminosity distribution, and comment on its implications. Using the distributions, we estimate the orbital velocity of the sun to be 240.15 ± 14 km/s, in excellent agreement with currently accepted values. Our calculation give the mass of the galaxy at $R = 21.1$ kpc to be $0.32 \pm 0.02 \cdot 10^{12}\ M_\odot$, which is well within modern measured ranges. We also hypothesize about the relationship between the mass and density distributions and Doppler broadening at differing longitudes.

Introduction — The Milky Way Galaxy is a spiral galaxy with a disk approximately 30 kpc (1 kpc = 3.086e19 meters) in diameter and a bright central bar region of contested size. [1]. As a result of the galaxy's scale and the Earth's location in it, directly observing its complete structure is far out of the reach of current science. However, measuring the velocity of orbiting bodies can allow us to calculate mass and mass distribution. In a circular Keplerian orbit, an object orbiting another body has velocity

$$V(R) = \sqrt{\frac{GM(R)}{R}} \tag{1}$$

where V is the velocity, R is the distance from the galactic center, G is the universal gravitational constant, $M(R)$ is the total mass $m_1(R) + m_2$, $m_1(R)$ is the mass inside the body's orbit as a function of radius, and m_2 is the body's own mass. Typically, $m_1(R) \gg m_2$, so $M(R) \approx m_{1(R)}$. Thus, we can solve Eq. 1 for the mass distribution

$$M(R) = \frac{V^2 \cdot R}{G} \tag{2}$$

As a result, measuring orbital velocities allows the characterization of mass distribution of the galaxy. It was hypothesized that mass was proportional to luminosity [2]; such a model predicts the Milky Way to have a massive center with some mass m_c orbited by comparably low-mass arms. In this case, $M(R)$ is a nearly constant m_c when $R > 0$, and the velocity decreases proportionally to the radius by

$$V(R) \propto \frac{1}{\sqrt{R}} \tag{3}$$

In order to measure the velocity distribution, we make use of the Small Radio Telescope (SRT) on the roof of Morse Hall. Radio waves' long wavelengths allow them to pass around interstellar dust regions that absorb or scatter the shorter-wavelength light other fields of astronomy rely on. Specifically, we observe the neutral-hydrogen line, also known as the 21-centimeter line, at a frequency of 1420.4 MHz. This frequency is so named because its wavelength is approximately 21 cm. The line results from the emission of a photon by neutral hydrogen atoms when their electron flips from spin-up state to spin-down state. For radiation the wavelength is $\lambda = \frac{hc}{\Delta E}$, where h is Planck's constant, c is the speed of light and ΔE is the energy difference between two states as defined by quantum hyperfine structure.[3] The probability of this transition is very low for a hydrogen atom: $2.9 \cdot 10^{-15} s^{-1}$ [4]. In other words, a given hydrogen atom has a 1 in $2.9 \cdot 10^{15}$ chance of emitting in any given second. However, galactic hydrogen clouds contain huge numbers of atoms and are nearly ubiquitous in the Milky Way; and so the 21-centimeter line can be observed reliably. [5]

Geometry – The layout of the problem is shown in Fig 2. V_0 and $V(R)$ are the velocities of the sun and a galactic cloud revolving around the galactic center (GC) in a plane with distance R_0 and R.

In the first quadrant ($0 < l < 90^o$) all the galactic clouds have positive radial velocity and the clouds outside solar orbit ($l > 90^o$) have negative radial velocity due to the motion of the sun. The maximum projected velocity is observed when the line of sight is tangential to the orbit of a cloud; we define this as terminal radial velocity V_m, given by

$$V_\mathrm{m} = V(R) - V_0\ sin(l) \tag{4}$$

with $R = R_0\ sin(l)$. The VERA experiment gives us very accurate solar parameters $R_0 = 8.05 \pm 0.45$ kpc and $V_0 = 238 \pm 14$ km/s . When the source is moving away from us with a positive velocity, there will be a negative shift in frequency due to the Doppler effect. The minimum frequency will give us the maximum projected velocity along the line of sight. Thus the most lowest frequency detected will correspond to the maximum source velocity, given by the equation

$$V_m = \frac{(1420.406 - f_{min}) \cdot c}{1420.406} - V_l \tag{5}$$

where V_m is the maximum velocity, c is the speed of

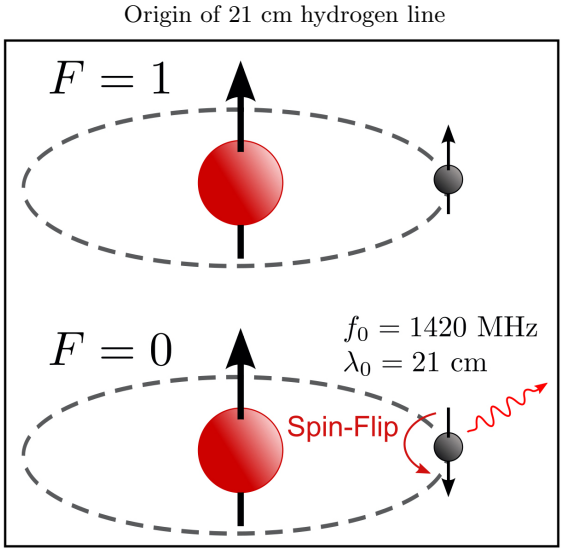

Figure 1: F=0 refers to parallel spin state for electron and the proton and F=1 state is for anti parallel. Due to the hyperfine structure F=1 state is more energetic than F=0, hence transition from higher state to lower release energy in terms of radiation with wavelength 21 cm.

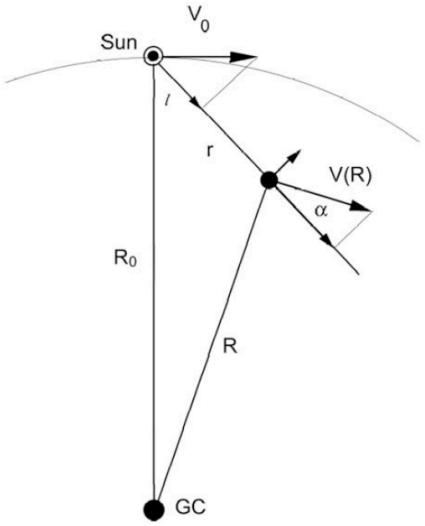

Figure 2: Assuming the sun is rotating around the Galactic Center (GC) at a distance R_0 with. velocity V_0. A Galactic cloud in the same plane as the sun and GC is at distance R moving with orbital velocity $V(R)$.

light, f_{min} is the minimum observed frequency, and V_l is the velocity of local standard of rest (VLSR). VLSR is a correction that accounts for the sun and earth's own velocity, which change relative to each galactic coordinate. The VLSR value is calculated by the SRT software and was recorded while collecting the data.

Methods – The raw data we collected from the SRT is in the form of antenna temperature as a function of frequency. The software sorts the data into 156 bins with bin width 0.0071825 MHz. The center of the distribution is 1420.4 MHz, and data was collected from all coordinates for 10 minutes. The mean of the time series in each bin was calculated to create the final frequency distribution for each galactic coordinate.

Table I: Galactic longitude, the minimum frequency obtained from the distribution, and is the maximum projected velocity obtained from equation 5.

GL	f_{min} (MHz)	VLSR(km/s)	V_m (km/s)
10	1419.85 ± 0.12	10.6	108.94 ± 1.66
20	1420.21 ± 0.12	9.5	99.48 ± 1.66
30	1419.90 ± 0.12	8.2	79.66 ± 1.66
40	1419.95 ± 0.12	6.7	70.6 ± 1.66
50	1420.00 ± 0.12	4.9	61.84 ± 1.66
60	1420.15 ± 0.12	3.1	31.96 ± 1.66
70	1420.25 ± 0.12	1.1	12.83 ± 1.66
80	1420.30 ± 0.12	-1.0	4.37 ± 1.66
90	1420.35 ± 0.12	-3.0	2.15 ± 1.66

Our next step was to plot the intensity against frequencies so we could find our minimum detected frequency. We then found the minimum frequency by looking for a shoulder in the curve above the noise threshold, then calculated the velocity using Eq. 5. See Table II for full results, Fig. 5 for plot examples.

Table II: Galactic longitude, galactic radius, and maximum orbital velocity obtained from equation. Already it can be seen the velocity does not decrease with radius.

GL (deg)	R (kpc)	$V(R)$ (km/s)
10	1.397 ± 0.960	150.27 ± 28.44
20	2.753 ± 0.925	180.88 ± 27.46
30	4.024 ± 0.871	198.66 ± 25.89
40	5.174 ± 0.798	223.58 ± 23.83
50	6.166 ± 0.713	244.16 ± 21.41
60	6.971 ± 0.622	238.07 ± 18.86
70	7.564 ± 0.537	236.48 ± 16.50
80	7.927 ± 0.474	238.76 ± 14.75
90	8.050 ± 0.450	240.15 ± 14.09

Error Analysis – We do not explicitly cover the calculation of uncertainty for every parameter. However, a brief overview is useful for understanding the results.

Some sources of uncertainty were the tools involved, especially the SRT and its software package. Others included the uncertainty in estimates we sourced for V_0 and R_0. Finally, there were the uncertainties in values we calculated, which necessitate the use of error propagation. See Table III for a complete list of instrument and estimate uncertainties.

Table III: Uncertainties in inputs not calculated or measured by the authors.

Uncertainty	Value	Source
δl	0.1207 rads	SRT beamwidth
δf	0.0078 MHz	SRT bin spacing
δV_{LSR}	0.1 km $\cdot$ s^{-1}	SRT software
δV_0	14 km $\cdot$ s^{-1}	VERA
δR_0	0.45 kpc	VERA

δl is somewhat of an outlier as it is defined as the calculated beamwidth

$$\delta l = \frac{1.22 \cdot \lambda}{D} \tag{6}$$

where λ is the wavelength of peak intensity and D is the telescope aperture diameter. However, relatively small uncertainties in λ and D result in the variability from coordinate to coordinate and uncertainty of the beamwidth being negligible once significant digits are considered.

For parameters calculated from the data, we use the general case error propagation equation for a function of many variables $F = F(x, y, z, ...)$

$$\delta F = \sqrt{\left(\frac{\partial F}{\partial x} \cdot \delta x\right)^2 + \left(\frac{\partial F}{\partial y} \cdot \delta y\right)^2 + \left(\frac{\partial F}{\partial z} \cdot \delta z\right)^2 + ...} \tag{7}$$

We will calculate δV_m as an example. Plugging Eq. 5 into Eq. 7 gives us

$$\delta V_m = \sqrt{\left(\frac{\partial V_{\mathrm{m}}}{\partial f_{\mathrm{min}}} \cdot \delta f_{\mathrm{min}}\right)^2 + \left(\frac{\partial V_m}{\partial V_{\mathrm{LSR}}} \cdot \delta V_{\mathrm{LSR}}\right)^2} \tag{8}$$

we then calculate

$$\frac{\partial V_m}{\partial f_{\mathrm{min}} \cdot \delta f_{\mathrm{min}}} = \frac{-c \cdot \delta f_{\mathrm{min}}}{1420.406} \tag{9}$$

and

$$\frac{\partial V_m}{\partial V_{LSR}} \cdot \delta V_{LSR} = -\delta V_{LSR} = -0.1 \text{ km} \cdot \text{s}^{-1} \tag{10}$$

plugging Eqs. 9 and 10 into 8 gives:

$$\delta V_m = \sqrt{\left(\frac{-c \cdot 0.0078}{1420.406}\right)^2 + (-0.1)^2} = 1.66 \text{ km} \cdot \text{s}^{-1} \tag{11}$$

for all V_m. Because minimum frequency and maximum velocity are linearly proportional, it is expected that the uncertainty in velocity depends only on the uncertainty in the frequency. Calculations for other parameter uncertainties proceeded using the same method of describing parameters in terms of variables with known uncertainties and applying Eq. 7.

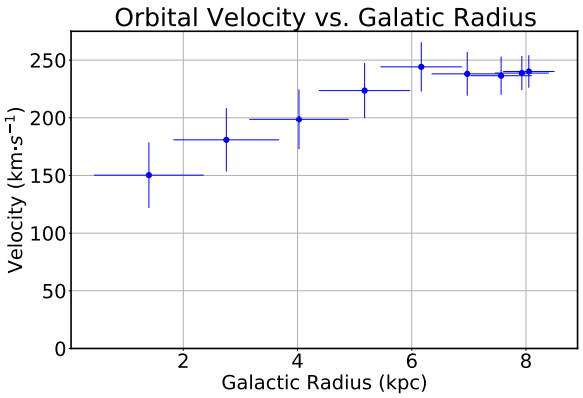

Figure 3: Orbital velocity of neutral hydrogen clouds versus their galactic radius. The curve does not follow the distribution anticipated by visible light observations, but increases linearly before flattening at larger radii.

Analysis – The orbital velocities and errors are shown in Table II Fig. 3. The velocities does not decrease with radius, but rather increase approximately linearly until about 6 kpc where the curve flattens. We calculate the velocity at G90 (which has a radius equivalent to the sun's) to be 240.15 ± 14.09 km/s, in excellent agreement VERA's 238 ± 14 km/s, and a "generally accepted" figure of ∼220 ± 20 km/s [6].

The rotation curve is clearly at odds with a luminosity-based mass distribution, and implies that there is some source of mass that is not being measured when observing luminosities. From Eq. 1, it is clear that when $V(R)$ is constant, $\frac{M(R)}{R}$ must also be constant, so $M(R) \propto R$. Using Eq. 2 to calculate the mass at each radius given the orbital velocity results in Fig. 4. As we expect from a flat rotation curve, the mass is directly proportional to radius. Linear regression of the mass-radius data calculated a slope of 0.1586, y-intercept of -0.1992 and an r^2 value of 0.987, indicating a very strong fit. Note that the fit is only useful for $R \geq 1.75$ kpc, as our velocity calculations do not include regions close to the galactic center. As a stretch test of our rudimentary model, we compare to the results of Watkins et. al 2019 [7]. The 2019 paper made use of proper motion data of Milky Way globular clusters from the European Sapce Agency's GAIA Mission [8] to estimate the galactic mass. Their more robust analysis results in $M(< 21.1 \text{ kpc}) = 0.21^{+0.04}_{-0.03} \cdot 10^{12} M_\odot$, while our regression predicts $M(< 21.1 \text{ kpc}) = 0.32 \pm 0.02 \cdot 10^{12} M_\odot$. Although the predictions are not in agreement, our estimation does fall within a range of 10^{11} to $2 \cdot 10^{12}$ kg cited

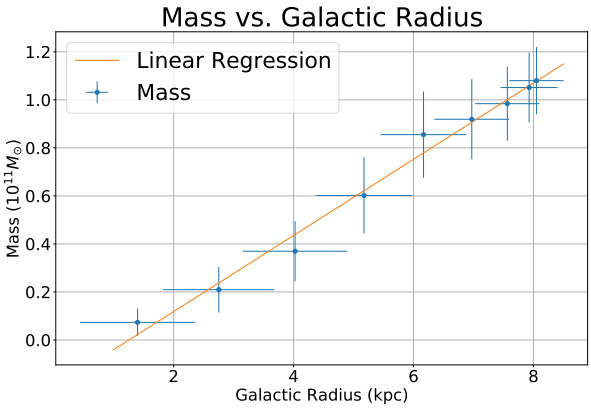

Figure 4: Mass v. Galactic Radius, calculated using Eq. 2 and the velocities and radii in Table II. The linear regression (slope = 0.1586, intercept = -0.1992) is not valid at small radii as no data was collected there.

by Watkins as common results.

It was noted that the frequency plots of GC and G10 show narrower, single peaks, while at longitudes $l \geq 20°$ there are two or more peaks separated by troughs that grow more prominent at higher latitudes. This effect is clearly seen in Fig. 5; the galactic center exhibits a tight peak with a very narrow split, while at G20 the trough has widened and a prominent shoulder peak has appeared The phenomenon is known as Doppler broadening, and it occurs when there is a distribution of velocities in the object's constituent particles. We hypothesize the break is the result of changes in the galaxy's average density. From our calculations, we know that $M(R) \propto R$, and since density is mass over volume, we find that the density function $D(R) \propto R^{-2}$. We confirmed this by plotting density against radius, with the assumption that the volume was spherical, seen in Fig 6.

G20's radius is approximately double that of G10, so the average density is lower by a factor of 4. That, combined with the gravitational force's identical falloff means that the higher longitude clouds are in weaker and less uniform gravitational fields, which allow for a greater distribution of particle velocities within the clouds.

Conclusion – In our work, we found that the rotation curve of the Milky Way is inconsistent with a mass distribution where mass is proportional to luminosity. Contrarily, we find that the mass distribution is linearly correlated with radius outside of the central region, resulting in a density distribution that follows R^{-2}. We also hypothesize that the jump in Doppler broadening is due to a combination of passing some critical density and the falloff of the gravitational force. Additionally, we find that our results are in excellent agreement with other published values for V_0 and even provided a total galactic mass well within an order of magnitude of recent

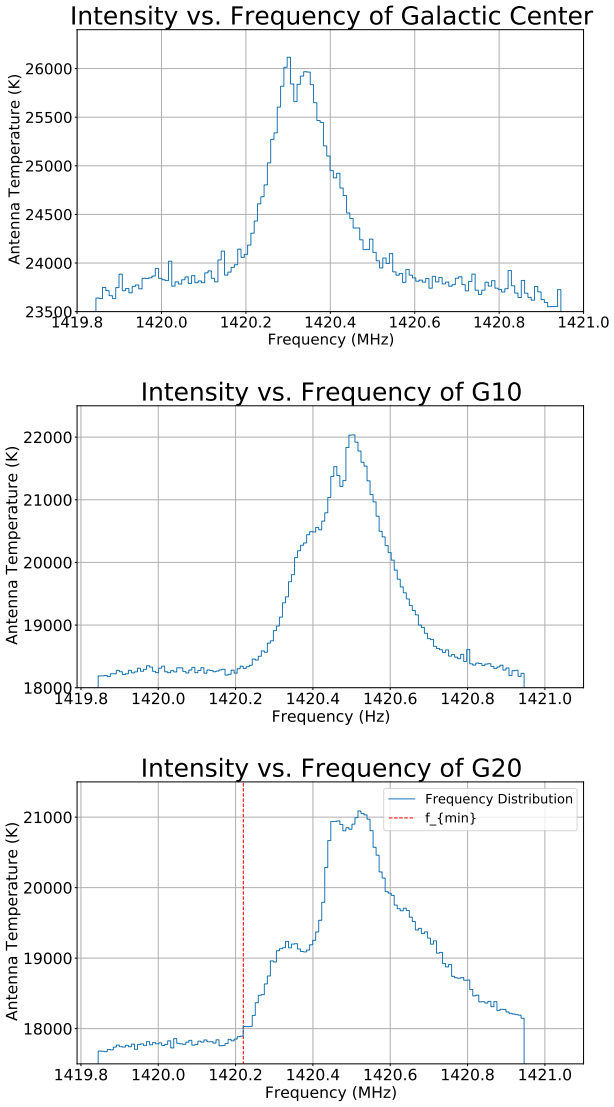

Figure 5: Plots of intensity vs frequency for the galactic center, G10, and G20. The Doppler broadening is subtle at GC and G10 but becomes much more pronounced at G20.

values, in spite of $R_{total} = 21.1$ kpc being well outside the radius where we collected data. Thus, we find the SRT to be an effective tool for conducting studies of the galactic rotation curve.

The data strongly contradicts the idea that mass and luminosity are correlated. Given that stars tend to dominate the mass of solar systems, this result implies that there is some source of mass (or at least, gravitational attraction) that is not being accounted for. It indeed was this discrepancy that lead Vera Rubin to make her calculations that became the driving force behind the modern study of dark matter.

Future work in this area of research is currently ongoing at many levels. With the SRT, possibilities in-

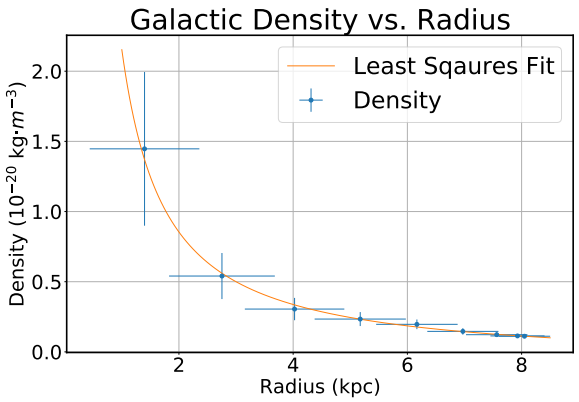

Figure 6: Plots of intensity vs frequency for the galactic center, G10, and G20. The Doppler broadening is subtle at GC and G10 but becomes much more pronounced at G20.

clude taking measurements at a wider variety of galactic longitudes to create a more detailed rotation curve and mass distribution. A more ambitious project would be to estimate the relative distribution of hydrogen in the galaxy. This could done by taking the difference of the average density distribution with the distribution of stars (through a luminosity distribution). A larger difference would imply a greater concentration of non-luminous matter, which could correlate to more neutral hydrogen.

Acknowledgement – The authors want to thank Professor John Gianforte and Professor Elena Long for their help and support in this study. And thanks, Vera.

* Corresponding author: hi1011@wildcats.unh.edu
† Corresponding author: epd1007@wildcats.unh.edu

[1] M. López-Corredoira, C. Allende Prieto, F. Garzón, H. Wang, C. Liu, and L. Deng, Astronomy Astrophysics **612**, L8 (2018).
[2] J. H. Oort, Astrophys. J. **91**, 273 (1940).
[3] H. I. Ewen, Nature (1951).
[4] Redshifted 21cm hydrogen line.
[5] P. M. Kalberla and J. Kerp, Annual Review of Astronomy and Astrophysics **47**, 27 (2009), https://doi.org/10.1146/annurev-astro-082708-101823.
[6] I. D. Karachentsev and D. I. Makarov, Astronomy Letters **22**, 455 (1996).
[7] L. L. Watkins, R. P. van der Marel, S. T. Sohn, and N. Wyn Evans, The Astrophysical Journal **873**, 118 (2019).
[8] T. Prusti, J. H. J. de Bruijne, A. G. A. Brown, A. Vallenari, C. Babusiaux, C. A. L. Bailer-Jones, U. Bastian, M. Biermann, D. W. Evans, and et al., Astronomy Astrophysics **595**, A1 (2016).